Title

CeO2 nanoparticles induce pulmonary fibrosis via activating S1P pathway as revealed by metabolomics

Authors

Cui, Li

Wang, Xiang

Zhao, Xinyuan

et al.

Publication Date

2022-08-01

DOI

10.1016/j.nantod.2022.101559

Peer reviewed

HHS Public Access

Author manuscript

Nano Today. Author manuscript; available in PMC 2023 August 01.

Published in final edited form as:

Nano Today. 2022 August ; 45: . doi:10.1016/j.nantod.2022.101559.

CeO_2 nanoparticles induce pulmonary fibrosis *via* activating S1P pathway as revealed by metabolomics

Li Cui[1,#], **Xiang Wang**[2,#], **Xinyuan Zhao**[3,#], **Bingbing Sun**[4], **Tian Xia**[2], **Shen Hu**[1]

[1]School of Dentistry, Jonsson Comprehensive Cancer Center, California NanoSystems Institute, University of California, Los Angeles, California 90095, United States

[2]Center for Environmental Implications of Nanotechnology (UC CEIN), California NanoSystems Institute, Division of NanoMedicine, Department of Medicine, University of California, Los Angeles, California 90095, United States

[3]Stomatological Hospital, Southern Medical University, Guangzhou, Guangdong 510280, China

[4]School of Chemical Engineering, Dalian University of Technology, Dalian 116024, China

Abstract

CeO_2 nanoparticles (NPs) have been shown to cause lung fibrosis, however, the exact underlying molecular mechanisms are poorly understood. In this study, we have conducted a mass spectrometry-based global metabolomic analysis of human bronchial epithelial BEAS-2B cells treated by CeO_2 NPs with different aspect ratios and assessed their toxicity on the bronchial epithelial cells by various cell-based functional assays. Although CeO_2 NPs at doses ranging from 12.5 μg/mL to 25 μg/mL displayed low cytotoxicity on the bronchial epithelial cells, the metabolomic analysis revealed a number of metabolites in the cellular metabolic pathways of sphingosine-1-phosphate, fatty acid oxidation, inflammation, *etc.* were significantly altered by CeO_2 NPs, especially those with high aspect ratios. More importantly, the robustness of metabolomics findings was further successfully validated in mouse models upon acute and chronic exposures to CeO_2 NPs. Mechanistically, CeO_2 NPs upregulated transforming growth factor beta-1 (TGF-β1) levels in BEAS-2B cells in an aspect ratio-dependent manner through enhancing the expression of early growth response protein 1 (EGR-1). In addition, both *in vitro* and *in vivo*

Corresponding authors: Shen Hu, Ph.D., M.B.A., School of Dentistry, Jonsson Comprehensive Cancer Center, California NanoSystems Institute, University of California, Los Angeles, California 90095, United States, Tel: 310-2068834, shenhu@ucla.edu.; Tian Xia, M.D., Ph.D., Center for Environmental Implications of Nanotechnology (UC CEIN), California NanoSystems Institute, Division of NanoMedicine, Department of Medicine, University of California, Los Angeles, California 90095, United States, Tel: 310-9833359, txia@ucla.edu.

[#]These authors equally contributed to this study.

CRediT authorship contribution statement

Shen Hu and Tian Xia conceived the study and designed the experiments. Li Cui, Xiang Wang, Xinyuan Zhao and Bingbing Sun performed the experiments. Shen Hu, Tian Xia, Li Cui and Xiang Wang analyzed the data and contributed to writing of the manuscript. All authors contributed to the manuscript and approved the submitted version.

Declaration of Competing Interest

The authors declare that they have no known competing financial interests or personal relationships that could have appeared to influence the work reported in this paper.

studies demonstrated that CeO_2 NPs significantly induced the expression of sphingosine kinase 1 (SHPK1), phosphorylated Smad2/3 and lung fibrosis markers. Moreover, targeting SPHK1, TGFβ receptor or Smad3 phosphorylation significantly attenuated the fibrosis-promoting effects of CeO_2 NPs, and SPHK1-S1P pathway exerted a greater effect on the TGF-β1-mediated lung fibrosis compared to the conventional Smad2/3 pathway. Collectively, our studies have identified the metabolomic changes in BEAS-2B cells exposed to CeO_2 NPs with different aspect ratios and revealed the subtle changes in metabolic activities that traditional approaches might have missed. More importantly, we have discovered a previously unknown molecular mechanism underlying CeO_2 NP-induced lung fibrosis with different aspect ratios, shedding new insights on the environmental hazard potential of CeO_2 NPs.

Keywords

CeO_2 nanorods/nanowires; aspect ratio; lung fibrosis; metabolomics; mass spectrometry; nanotoxicity

Introduction

Nanomaterials with high aspect ratios have been widely used in nanodevices owing to their unique chemical, mechanical, electric, and optical properties [1, 2]. However, there is growing concern about their potential adverse health and environmental effects. In addition, increasing evidences have demonstrated that the aspect ratio of nanoparticles (NPs) is closely associated with their biological functions and activities [3–5]. For instance, we have previously revealed that CeO_2 NPs with a higher aspect ratio induced more toxicity in the lung and gastrointestinal tract [6]. However, the underlying molecular mechanisms were not fully discovered. The pulmonary exposure and risk potential of CeO_2 NPs is based on the application of Ce containing materials, including high aspect ratio CeO_2 NPs, as additives for fuel combustion, for instance as a diesel engine catalyst to reduce the exposure of diesel exhaust, surface polishing/planarization, corrosion protection, solar cells and biomedical devices [6–13]. Because CeO_2 NPs with high aspect ratios are extensively applied in manufacturing commercial products, it is of great importance to understand the intrinsic molecular events that drive the nanotoxicity of CeO_2 NPs with high aspect ratios.

The rapid development of high-throughput omics technologies such as genomics, transcriptomics, proteomics, and metabolomics has contributed significantly to dissecting the network of genes, transcripts, proteins, and metabolites globally within a biological system[14]. Metabolites are the intermediates or end products of metabolism that play a crucial role in maintaining essential cellular functions and phenotypes [15, 16]. Numerous evidences have demonstrated that metabolites not only affect the cellular signals by interacting with proteins or modulating protein activity *via* post-translational modifications but also in turn alter the microenvironment that they are produced or secreted [17]. Therefore, it is important to ascertain the metabolites and metabolic pathways that are associated with or determine the specific phenotype traits. The untargeted mass spectrometry (MS)-based metabolomics can quantitatively measure a broad range of metabolites present in an extracted sample subjected to pathophysiological stimuli or genetic modification.

We previously have demonstrated that untargeted or targeted metabolomics, based on liquid chromatography with tandem mass spectrometry (LC-MS/MS), are highly robust and accurate for identifying metabolic signatures for cancer stem cells, discovering novel molecular mechanisms of oral/head and neck cancer, or detecting gout disease [18–20].

In this study, we have demonstrated that LC-MS-based metabolomics was more sensitive to detect subtle cellular changes induced by CeO_2 NPs compared to the traditional cell-based functional assays. In addition, the *in vitro* metabolomic findings were robustly validated *in vivo* with mouse models upon acute and chronic exposures to CeO_2 NPs. More importantly, based on the metabolomic findings, we have revealed a previously unknown mechanism for the induction of lung fibrosis caused by CeO_2 NPs in an aspect ratio-dependent manner.

Results

Physicochemical characterization of CeO_2 NPs

As shown by transmission electron microscopy (TEM) analysis in Figure 1A, all the three CeO_2 NPs were rod- or wire-shaped with different aspect ratios. The particle size and ζ-potential of the CeO_2 NPs in deionized (DI) water and complete cell culture medium were measured (Figure 1B). The results showed that all the three CeO_2 NPs agglomerated in DI water, with hydrodynamic sizes of 231.4 ± 12.0, 651.3 ± 72.1, 978.8 ± 85.5 nm, respectively. Their ζ-potential values were −28.7 ± 1.1, −23.4 ± 3.7, −31.6 ± 1.9 mV, respectively. Similarly, the hydrodynamic sizes of all the three CeO_2 NPs in complete cell culture medium were 578.1.4 ± 97.8, 749.3 ± 116.5, 776.5 ± 93.4 nm, respectively. Their ζ-potential values were −11.1 ± 2.6, −15.3 ± 1.3, −9.7 ± 0.7 mV, respectively. The colloidal stability of CeO_2 NPs in DI water and BEGM was then evaluated. The Suspension stability index in cell culture media could serve as a reflection of the sedimentation rate of the NPs. As shown in Figure S1, CeO_2 NPs #1 displayed the highest stability with ca. 97 % remaining after 20 h, followed by CeO_2 NPs #2 and #3, which exhibited similar level of stability in BEGM. TEM was also used to investigate the interaction of CeO_2 NPs with BEAS-2B cells. The CeO_2 NPs with difffent aspect ratios could be taken up by BEAS-2B cells. Interestingly, CeO_2 # 1 NPs were internalized into membrane-lined subcelluar compartments in BEAS-2B cells (Figure 1C). The dissolution of CeO_2 NPs in two different simulated biological fluids namely the Gamble's solution and phagolysosomal simulant fluid (PSF) [21] was determined. Gamble's solution has a pH of 7.4 and is used to simulate the interstitial fluid deep within the lung; whereas PSF has a pH of 4.5 and is analogous to the fluid with which the CeO_2 NPs would come into contact after phagocytosis by alveolar and interstitial macrophages in the lung. The results showed no significant dissolution of all the three CeO_2 NPs in both simulant fluids (Figure S2). Inductively coupled plasma optical emission spectroscopy (ICP-OES) was used to quantify the uptake of CeO_2 NPs by BEAS-2B cells. The data showed that there was not statistical difference among the three different CeO_2 NPs post-exposed to the cells *in vitro* (Figure S3).

Functional cellular assays of CeO2 NPs-treated BEAS-2B cells

Various cell-based functional assays were performed to investigate the effects of CeO_2 NPs exposure on BEAS-2B cells. The EdU assay showed that the percentage of cells with S

phase DNA content changed little in the BEAS-2B cells exposed to CeO_2 NPs with different aspect ratios (Figure 2A). The flow cytometry revealed that the cell cycle distribution was similar between the untreated cells and those treated with different types of CeO_2 NPs (Figure 2B). Likewise, immunofluorescence analysis demonstrated that the fluorescence intensity of proliferating cell nuclear antigen (PCNA), a well-established cell proliferation marker, altered slightly in the BEAS-2B cells exposed to CeO_2 NPs (Figure 2C). Similar findings were observed with the MTS assay (Figure 2D). In addition, the GSH assay did not reveal significant change in GSH level in the BEAS-2B cells exposed to CeO_2 NPs (Figure 2E). Lastly, no significant alteration in the levels of inflammatory cytokines, IL-6, IL-8 and IL-1β, and the mitochondria potential were found in the cells exposed to different types of CeO_2 NPs (Figure 2F and 2G).

Metabolomic analysis of CeO_2 NP-treated BEAS-2B cells

LC-MS based metabolomic analysis of CeO_2 NPs-treated and untreated BEAS-2B cells was performed to identify significantly altered metabolites in the cells treated by three different types of CeO_2 NPs (CeO_2 NPs #1, CeO_2 NPs #2, CeO_2 NPs #3). Seven study groups, untreated control, CeO_2 NPs #1 (high dose, 25 μg/mL; low dose, 12.5 μg/mL), CeO_2 NPs #2 (high dose, 25 μg/mL; low dose, 12.5 μg/mL), CeO_2 NPs #3 (high dose, 25 μg/mL; low dose, 12.5 μg/mL), were included for the metabolomic analysis and each group included six independent samples (6 biological replicates). A total of 8885 metabolic features were found to be present in the cellular metabolomic samples of the 7 study groups, and 279 metabolites were identified in total. Volcano plots were produced to display the metabolic features between each CeO_2 NP treatment and control groups. Red or green dots in the volcano plots represented significantly increased (q value <0.05; ratio ≥ 1.200) or decreased metabolites (q value <0.05; ratio ≤ 0.833), respectively. As shown in Figure 3A, the metabolomic analysis allowed the detection of 1049 (533 increased and 516 decreased), 2012 (1203 increased and 809 decreased), 1431 (720 increased and 711 decreased) significantly altered metabolic features in the BEAS-2B cells treated with CeO_2 #1, CeO_2 #2, and CeO_2 #3 NPs, respectively, when compared to the untreated cells. Heatmaps were used to visualize the pattern of significantly changed metabolites between each CeO_2 NP treatment and control group (Figure 3B). The number of identified metabolites with significant changes between each of the three two-group comparisons were shown in Figure 3C, which were 105 (62 increased and 43 decreased, CeO_2 NPs #1), 200 (155 increased and 45 decreased , CeO_2 NPs #2), and 153 (93 increased and 60 decreased , CeO_2 NPs #3), respectively. These identified metabolites were listed in Supplementary Tables 1–3. The number of commonly and differentially altered metabolites among the three types of CeO_2 NPs with different aspect ratios was presented in Figure 3D and 3E. A total of 43 metabolites were shared among the three CeO_2 NP-treated groups.

The relative changes in a panel of amino acids, nucleosides, nucleotides, tricarboxylic acid (TCA) cycle intermediates, glycolytic metabolites, sphingosine-1-phosphate (S1P) pathway metabolites, carnitines and inflammatory metabolites in the BEAS-2B cells, when exposed to three different CeO_2 NPs (CeO_2 NPs #1, CeO_2 NPs #2 and CeO_2 NPs #3), were depicted in Figures 4 and 5. Most of these metabolites were significantly increased in the cells treated with CeO_2 #2 or CeO_2 #3 NPs when compared to the untreated cells. However, no

significant changes in most of these amino acids were found in the cells exposed to CeO_2 #1 NPs, which had the lowest aspect ratio (Figure 4A–4C). Interestingly, we found that all the three CeO_2 NPs significantly increased the levels of acylcarnitines, the metabolites in the S1P pathway, and PGE2 in BEAS-2B cells (Figure 5A–5B). Heatmaps were also produced to visualize the differential levels of representative metabolites in the cells treated by the three types of CeO_2 NPs at high and low doses. Most of the representative metabolites shown in Figure 5C–5E were altered by CeO_2 NPs in a dose-dependent manner.

In vivo validation of the significantly altered metabolites in the mouse model upon acute exposure to CeO_2 NPs

The C57BL/6 mice were exposed to the three different CeO_2 NPs by oropharyngeal aspiration and the lung tissues were harvested after 40 h of exposure for enzymatic assays of the representative metabolites identified by the *in vitro* metabolomic analysis. The doses we chose for the *in vivo* exposure were 0.5 (low dose) and 2.0 (high dose) mg/kg. The presence of lung inflammation was confirmed by the histology results. CeO_2 #2 and CeO_2 #3 NPs at high aspect ratios induced focal neutrophil infiltration in the bronchioles and alveoli areas, along with alveolar wall thickening, whereas CeO_2 #1 NPs with a low aspect ratio had less noticeable effects at either low or high dose (Figure 6A). As shown in Figure 6B, enzymatic assays demonstrated that the levels of S1P, PGE2, and arachidonic acid were significantly increased in the mouse lung tissues subjected to the exposure of CeO_2 NPs in an aspect ratio- and a dose-dependent manner.

Chronic exposure to CeO_2 NPs induces lung fibrosis in the mouse model

Our *in vivo* studies with the mouse model demonstrated that long-term (44 days) exposure of CeO_2 NPs, especially CeO_2 #2 or CeO_2 #3 NPs, induced collagen formation in the mouse lung tissues. The lung tissues treated with SiO_2 were used as the positive controls for the comparison (Figure 7A). Interestingly, the levels of TGF-β1, a known pulmonary fibrosis inducer, were founded significantly increased in the bronchoalveolar lavage fluids (BALF) from CeO_2 NP or SiO_2 NP treated mice (Figure 7B). The total collagen levels in the lung were also significantly upregulated by all three CeO_2 NPs (Figure 7C). However, due to its lowest aspect ratio, a much significantly higher uptake of CeO_2 NPs #1 (>13 fold) by the mouse lung tissue cells was observed than the uptake of CeO_2 #2 or CeO_2 #3 NPs (Figure 7D). Therefore, the normalized levels of lung collagen to the uptake of CeO_2 NPs were 11.4-16.8 fold higher in the mice exposed to CeO_2 #2 and CeO_2 #3 NPs than those exposed to CeO_2 #1 NPs (Figure 7E). The *in vitro* metabolomic findings were further validated in the mouse model chronically exposed to CeO_2 NPs. As shown in Figure 7F–7G, the enzymatic assays demonstrated the levels of alanine, asparagine, glutamine, histidine, serine, S1P, PGE2, lactate, arachidonic acid, and fumaric acid were all significantly increased in the mouse lung tissues exposed to CeO_2 NPs.

Upregulation of early growth response 1 (EGR1) in BEAS-2B cells by CeO_2 NPs

We demonstrated that EGR1, an upstream regulator of TGF-β1, was upregulated by CeO_2 NPs in BEAS-2B cells. As expected, in BEAS-2B cells, the CHIP-qPCR showed that the promoter fragments of TGF-β1 was significantly enriched by the EGR1 antibody, and EGR1 depletion significantly reduced the enrichment (Figure 8A). The luciferase reporter assay

revealed that EGR1 directly induced the promoter activity of TGFB1 gene in BEAS-2B cells (Figure 8B). Western blot analysis showed that the expression levels of EGR1 and TGF-β1 were significantly increased in the BEAS-2B cells exposed to CeO_2 NPs in an aspect ratio dependent manner, and EGR1 knockdown by siRNA markedly reduced the expression of TGF-β1 (Figure 8C). Meanwhile, EGR1 knockdown also significantly reduced the TGF-β1 levels in the culture media from the BEAS-2B cells treated with CeO_2 NPs (Figure 8D).

CeO_2 NPs induces lung fibrosis through TGF-β1-SPHK1-S1P and TGF-β1-SMAD signaling pathways

Of note, the levels of S1P were significantly altered by CeO_2 NPs in an aspect ratio-dependent manner in the lung fibrosis mouse model induced by chronic CeO_2 NP treatment (44 days, Figure 7G). As S1P has been shown to regulate tissue fibrosis, we speculated that the significant alteration in S1P metabolic pathway might be crucial for CeO_2 NPs-induced lung fibrosis. As shown in Figure 9A, the expression level of sphingosine kinase 1 (SPHK1), a critical metabolic enzyme for S1P production and secretion, was significantly induced by CeO_2 NPs in an aspect ratio dependent manner. The levels of pSmad2 and pSmad3 were also significantly increased in the BEAS-2B cells following CeO_2 NPs exposure (Figure 9A). As shown Figure S4, EGR1 knockdown significantly suppressed the expression levels of SPHK1, pSmad2 and pSmad3 in BEAS-2B cells exposure to CeO_2 NPs. These findings supported that CeO_2 NPs active TGF-β1-SPHK1-S1P pathway and TGF-β1-Smad pathway by regulating EGR1 in BEASE-2B cells. The immunofluorescence analysis demonstrated that the expression of fibrosis markers COL1A and α-SMA were dramatically upregulated by CeO_2 NPs in an aspect ratio-dependent manner (Figure 9B). More importantly, the expression of EGR1, SPHK1, pSmad2, and pSmad3 were significantly increased in the lung tissues of CeO_2 NP treated mice in an aspect ratio-dependent manner (Figure 10). As shown in Figure 11 A, blocking the interaction between TGF-β1 and TGF-β receptor (TGFBR) markedly decreased the expression of SPHK1, pSmad2, and pSmad3 in the BEAS-2B cells exposed to CeO_2 #3 NPs, indicating that SPHK1 and pSmad2/pSmad3 might be the crucial downstream effectors for mediating CeO_2 NP/TGF-β1 induced lung fibrosis. Interestingly, blocking TGF-β1/TGFBR binding almost completely reduced the enhancing effects of CeO_2 #3 NPs on the expression of COL1A and α-SMA in BEAS-2B cells. In addition, targeting SPHK1 with SKI II had a more attenuation effect on the expression of COL1A and α-SMA, when compared to targeting Smad3 phosphorylation (Figure 11B), suggesting that SPHK1-S1P pathway exerted a greater effect on the TGFβ-1-mediated lung fibrosis than the conventional Smad2/3 pathway. The proposed model for CeO_2 NP-induced lung fibrosis was depicted in Figure 12.

Discussion

In this study, we have shown that LC-MS-based metabolomics is a highly sensitive and efficient methodology for the assessment of nanotoxicity. Although no significant changes of the cell functions/phenotypes were observed based on traditional cell-based functional assays, the metabolomic analysis revealed distinct metabolome alterations in human bronchial BEAS-2B epithelial cells exposed to CeO_2 NPs with different aspect ratios. Significantly elevated metabolites in the BEAS-2B cells, when exposed to high-

dose CeO_2 NPs, included amino acids, nucleotides, nucleotides, *etc.*, which are building blocks for the cell proliferation and subsequent fibrosis. In addition, the changes in metabolites of the TCA cycle and glycolysis pathway might contribute to the metabolic reprogramming of BEAS-2B cells, which promoted epithelial-mesenchymal transition and consequently fibrosis. Meanwhile, inflammatory metabolites (PGE2, arachidonic acid), the metabolites of fatty acid oxidation as well as the metabolites of the S1P pathway were significantly increased by high-dose CeO_2 NPs. The metabolomic analysis results that CeO_2 nanorods with a higher aspect ratio tend to induce more severe inflammatory responses was consistent with our previous findings [6, 22]. The persistent inflammatory environment might contribute to the formation of fibrotic tissues. A dose-dependent effect of CeO_2 NPs on the levels of certain representative cellular metabolites was observed. More importantly, CeO_2 NPs with a higher aspect ratio induced more significant alterations in the cellular metabolites than those with a lower aspect ratio. In this regard, CeO_2 NPs with a high aspect ratio appear to pose higher nanotoxicity to human bronchial epithelial cells than those spherical CeO_2 NPs with a low aspect ratio. In addition, representative metabolites with significant alterations were validated in the mouse models upon acute and chronic exposures to CeO_2 NPs, suggesting that the *in vitro* metabolomic alterations due to the exposure of CeO_2 NPs might be used to predict the toxicological effects of CeO_2 NPs *in vivo*.

It is well-established that activation of TGF-β1 signaling is critical for tissue fibrosis [23–25]. Thus, it is not surprising that the level of TGF-β1 was significantly increased in the BEAS-2B cells or the lung tissues from the mice exposed to CeO_2 NPs. Longer CeO_2 nanowires tend to bundle together, which might significantly hinder the cellular uptake of CeO_2 #2 and CeO_2 #3 NPs. However, the total amount of collagen was still slightly higher in the lung tissues exposed to CeO_2 #3 NPs compared to those exposed to CeO_2 #1 NPs, and the collagen level was similar in the lung tissues derived from CeO_2 #2 NP and CeO_2 #1 NP treated mice. These findings strongly demonstrate that CeO_2 NPs with higher aspect ratios are more efficient in inducing lung fibrosis compared to those with a lower aspect ratio. We also provided compelling evidence showing that CeO_2 NPs enhanced the expression of EGR1 in an aspect ratio-dependent manner both *in vitro* and *in vivo*, and EGR1 was an important upstream regulator for TGF-β1 signaling. However, the detailed molecular mechanisms for EGR1 upregulation following CeO_2 NPs exposure needs further investigation.

The metabolomic analysis revealed that the metabolites in the S1P metabolic pathway in BEAS2B cells were siginificantly upregulated by CeO_2 NPs. S1P is a bioactive metabolite involved in the regulation of many physiological and pathological processes [26] Changes in S1P levels have been linked to a number of disease conditions such as inflammation, cancer, and obesity [27–29]. Previous studies have shown that the S1P signaling may promote pulmonary fibrosis [30, 31]. Of note, we were the first to demonstrate that the levels of S1P were significantly altered by CeO_2 NPs in an aspect ratio-dependent manner both *in vitro* and *in vivo*. These findings further support the robustness of metabolomics for identifying the important metabolites that might be mediating CeO_2 NP-induced nanotoxicity. As expected, the expression of SPHK1, which is an important metabolic enzyme that directly regulates the production and secretion of S1P, was upregulated by CeO_2 NPs in an aspect ratio-dependent manner. Blocking the interaction between TGF-β1 and its receptor TGFBR

not only significantly reduced the expression SPHK and the phosphorylation of Smad2 and Smad3, but also almost completely obliterated the fibrosis-promoting effects of CeO_2 NPs, indicating that SPHK1-S1P pathway and SMAD signaling pathway are both downstream effectors of TGF-β1. More importantly, SPHK depletion was more effective for reducing the CeO_2 NP/EGR1/TGF-β1-induced fibrosis compared to targeting SMAD signaling, suggesting CeO_2 NPs mainly promotes the lung fibrosis in an aspect ratio dependent manner through the TGF-β1/SPHK1/S1P pathway rather than the conventional TGF-β1-SMAD pathway. Considering the fibrosis promoting effects of CeO_2 NPs, it should be pointed out that there are several "safer by design" strategies that could be implemented to improve material safety, including shortening the length or lower the aspect ratio [6], coating the surface with phosphonate [32, 33], polymers or co-polymers, such as Pluronic F108 and Pluronic F87 [34–37], etc., and doping the NPs with other inert elements [38–42]. Our study has provided robust evidence for demostrating the powerfulness of metabolomics for predicting nanotoxicity in mammalian system. Since both Zebrafish and *Caenorhabditis elegans* (worm) have been used for nanotoxicity studies [43, 44], it would be feasible to utilize metabolomics to study nanotoxicity in these model organisms.

Conclusions

Collectively, we have demonstrated that LC-MS-based metabolomics is not only highly sensitive for identifying subtle metabolomic changes induced by CeO_2 NPs that conventional functional assays may miss but also robust for predicting the nanotoxicity in mouse models upon acute and chronic exposures to CeO_2 NPs. In addition, EGR1 is identified as an important upstream regulator of TGF-β1 in CeO_2 NP induces fibrosis. More importantly, we have discovered a previously unknown molecular mechanism that CeO_2 NPs mainly promotes lung fibrosis in an aspect ratio dependent manner through the TGF-β1/SPHK1/S1P pathway in addition to the conventional TGF-β1-SMAD pathway, which provide novel insights into the hazardous potential of CeO_2 NPs.

Materials and methods

Materials

CeO_2 NPs were provided in powder form from the Division of NanoMedicine, Department of Medicine, University of California, Los Angeles. The BEAS-2B bronchial epithelial cells were maintained in the bronchial epithelial growth medium (BEGM, Lonza, Mapleton, IL, USA). The ELISA kits for human TGF-β1, IL-6, IL-1β, and IL-8 were purchased from the BD Biosciences (San Diego, CA, USA), and the kits for the CellTiter 96® AQ_{ueous} MTS and GSH-Glo glutathione assays were obtained from Promega (Madison, WI, USA). The assay kits for alanine, asparagine, glutamine, serine, lactate and fumaric acid were purchased from Abcam (Cambridge, UK). The histidine, sphingosine-1-phosphate, PGE2, arachidonic acid ELISA kits were purchased from MyBioSource (San Diego, CA, USA).

Physicochemical characterization of CeO_2 NPs

The CeO_2 nanoparticle (NP) dry powder was weighed and then suspended in deionized water by vortexing and bath sonication (Branson, model 2510, 100 W output power; 42

kHz frequency) to yield a stock solution of 5 mg/mL as previously described [6, 22]. This stock suspension was used as the stock solution for further dispersion in cell culture media. An appropriate amount of the stock solution was added to the cell culture medium to obtain a final concentration of 12.5 (low dose) or 25 (high dose) μg/mL. The diluted NP suspension in the cell culture medium was vortexed (15 s) and sonicated (15 min) in a water bath sonicator, followed by another 15 s vortex to obtain the final suspension. A ZetaPALS (Brookhaven Instruments Corporation, Holtsville, NY, USA) was used to measure the size and zeta-potential of the NP suspension. The primary length and diameter of CeO_2 nanomaterials were determined by using transmission electron microscopy (TEM, JEOL JEM 2010, JEOL USA, Inc., Peabody, MA, USA), while the suspended particles were used for assessment of hydrodynamic size and surface charge.

Cell Culture

The BEAS-2B cells were obtained from the American Type Culture Collection (ATCC, Manassas, VA) and maintained in the bronchial epithelial growth medium (BEGM, Lonza, Mapleton, IL, USA) supplemented with growth factors from the SingleQuot kit (Lonza) at 37 °C in a humidified atmosphere containing 5% CO_2.

EdU (5-Ethynyl-2′-deoxyuridine) assay

The Click-iT™ EdU cell proliferation kit for imaging (Invitrogen) was used to assess cell proliferation according to the manufacturer's recommended protocols. Briefly, after exposure to CeO_2 NPs with different aspect ratios, the cells were incubated with 10 μM EdU for 2 h at 37 °C. Followed by fixation with 3.7% formaldehyde and permeabilization with 0.5% Triton X-100, the cells were incubated with freshly prepared Click-iT reaction cocktail in the dark for 30 min at room temperature, and then Hoechst 33342 dye was used for visualization of the nucleus. Images were taken with a confocal laser scanning microscope (Olympus, Center Valley, PA, USA).

Flow cytometry

The BEAS-2B cells with indicated treatments were trypsinized and fixed in 70% ice-cold ethanol at −20°C overnight. Followed by washing twice with PBS, 1 μL FxCycle™ Violet Stain (Invitrogen) was added to each sample, and the samples were then incubated in the dark at room temperature for 30 min. The Attune NxT Flow Cytometer (Invitrogen) was used to analyze the cellular samples.

MTS assay and measurement of mitochondrial potential

MTS assays were carried out with the CellTiter 96® AQ_{ueous} MTS (Promega, Madison, WI, USA). Ten thousand cells in 100 μL of medium were plated in each well of a 96-well plate (Costar, Corning, NY, USA) for overnight growth. The medium was removed and the cells were treated for 24 h with 100 μL of a series of NP suspensions to yield the final concentrations of 25 μg/mL. For the MTS assay, the cell culture medium was removed, and the cells were washed twice with PBS before the incubation with 100 μL of culture medium containing 16.7% of MTS stock solution for 1 h at 37 °C. The supernatant was transferred to a new 96-multiwell plate and centrifuged at 2000g for 10 min to spin down

the cell debris and NPs. Eighty microliters of the supernatant was removed from each well and transferred into a new 96-well plate. The absorbance of formed formazan was read at 490 nm on a SpectraMax M5 microplate spectrophotometer (Molecular Devices, Sunnyvale, CA). The measurements of mitochondrial potential were performed using a method described previously [45].

Determination of Intracellular GSH

The intracellular GSH level was measured with the GSH-Glo assay kit (Promega) according to the manufacturer's protocol. After CeO_2 NP exposure, the supernatant was discarded and 100 μL of GSH-Glo reaction buffer containing luciferin-NT and glutathione S-transferase was added to each sample. Followed by incubation at room temperature with constant shaking for 30 min, the samples were treated with 100 μL of luciferin D detection reagent for 15 min. The luminescent signal was detected with a Synergy HT microplate reader (BioTek Instruments, Winooski, VT, USA).

ELISA of IL-6, IL-8, IL-1β and TGF-β1

The culture media derived from CeO_2 NP treated cells were collected and the cell debris were removed by centrifugation. The levels of IL-6, IL-8, IL-1β and TGF-β1 in the samples were quantified with ELISA kits (BD Biosciences) according to the manufacturer's instructions. The signals were recorded using a microplate reader (BioTek).

Validation of metabolites with enzymatic assays or ELISAs

Representative metabolites including S1P, PGE2, arachidonic acid, alanine, asparagine, glutamine, histidine, serine, lactate and fumaric acid were further validated in the lung tissues of mice exposed to CeO_2 NPs. The assays were performed with commercially available kits according to the manufacturers' assay protocols. The levels of validated metabolites were determined based on the calibration curves of included standards of the kits.

Sample preparation for metabolomic analysis

BEAS-2B cells were suspended in the BEGM medium at a density of 5×10^5/mL and then plated on six-well plates with 2 mL BEGM per well. After overnight incubation at 37 °C, the culture media were replaced with NP suspensions in the BEGM at a concentration of 12.5 or 25 μg/mL, followed by 6 h incubation; extraction of metabolites was then performed according to our previous method [45]. Briefly, the cells were quickly washed twice with ice-cold PBS in a cold room and then quickly rinsed with Milli-Q water. After removal of Milli-Q water, the cells were flash frozen with liquid N_2. Afterwards, 1.0 mL of ice-cold 90% MeOH/10% $CHCl_3$ was immediately added to each well, and the cells were scraped with a cell scraper. Extracts were immediately transferred to microcentrifuge tubes and pelleted at 4 °C for 3 min at 16,000*g*. Supernatants were then transferred to new microcentrifuge tubes and vaccum dried for LC-MS analysis. All experiments were performed with six biological replicates (n = 6 each group).

LC-MS/MS

Untargeted global metabolomic analysis was performed with a similar LC-MS/MS method described previously [45]. Briefly, the extracted metabolites were separated using an ACQUITY UPLC system (Waters, Milford, MA, USA), with a reversed phase C18 column (ACQUITY UPLC HSS T3, 100 Å, 1.8 μm, 2.1 × 100 mm, Waters), and then detected using a Xevo G2-XS quadrupole time-of-flight (qTOF) mass spectrometer (Waters) in both positive and negative electrospray ionization (ESI) modes. The LC flow rate, injection volume, mobile phase compositions and gradient elution conditions as well as the experimental setting for ESI and MS data acquisition had been described before in details [45].

A QC sample was prepared by pooling the same volume of each cellular metabolomic sample (n = 42 samples in total, 7 groups, 6 samples/group), and the pooled QC sample was analyzed before, during and after running the cellular metabolomic samples to evaluate the stability of the LC-MS instrument. The extracted ion chromatographic peaks of eight abundant ions were selected for method evaluation and validation. The reproducibility of the method was evaluated based on 14 replicate runs of the QC sample, and the RSD for the corrected retention times was below 0.5%. The QC sample was run six times before the first cellular metabolomic sample, once after every seven cellular metabolomic samples, and three times after the last (42nd) metabolomic sample to prevent errors due to the matrix effect and day-to-day instrument variations. These QC sample runs were also used to calibrate for the drift in the retention time of all analyses.

Analysis of metabolomic data

Analysis of the metabolomic data was performed using the same method described previously for metabolite identification and quantification [45]. In the univariate analysis, the p-values were acquired with a Student's t test and adjusted using the false discovery rate method to obtain the q-values for each metabolite. A corrected p-value (q-value) < 0.05 was deemed as statistically significant. Fold change (FC, $\log_2$-scaled) was used to show the alterations of metabolites between groups, and differential metabolites were defined based on q-values < 0.05 and FC ≥ 1.200 or ≤ 0.833. The FC values and q-values for metabolites were also presented as volcano plots. Heatmaps were generated using the Morpheus software from the Broad Institute (https://software.broadinstitute.org/morpheus/).

Assessment of toxicological responses in the mouse lung

Male C57Bl/6 mice (8 weeks old) were purchased from the Charles River Laboratories (Hollister, CA, USA). The animals were housed under standard laboratory conditions established by the UCLA and NIH Guidelines for the Care and Use of Laboratory Animals in Research (DHEW78-23). The experimental protocol was approved by the Chancellor's Animal Research Committee at UCLA and includes standard operating procedures for animal housing (filter-topped cages; room temperature at 23 ± 2 °C; 60% relative humidity; 12 h light, 12 h dark cycle) and hygiene status (autoclaved food and acidified water). The test animals (6 mice/per group) were treated with CeO_2 NPs by an oropharyngeal aspiration as described previously [46, 47]. Briefly, the mice were anesthetized by intraperitoneal injection of ketamine (100 mg/kg) and xylazine (10 mg/kg). With the anesthetized animals

held in a vertical position, 50 μL suspensions containing CeO_2 NPs at 10 or 40 μg in PBS (equivalent to 0.5, 2.0 mg/kg) were instilled at the back of the tongue to allow aspiration in the lung. The animals in the control group received the same volume of PBS. The positive control group in each experiment was composed of animals receiving 5.0 mg/kg quartz (Min-U-Sil). The mice were sacrificed after 40 h (acute) or 44 days (chronic) of exposure, and BALFs and lung tissues were collected. The BALF was used to perform measurement of cytokine and growth factor levels by ELISA assays. The left lobe of the lung from each mouse was stained with hematoxylin/eosin or Masson's trichrome for histological analysis; while the right three lobes was homogenized with a Tissuemiser homogenizer (Fisher Scientific) for the measurement of the total collagen content, Ce element content and levels of metabolites of interest.

Sircol assay for total collagen production in lung tissue

The right lobes of each lung were suspended in PBS at ~50 mg tissue/mL and homogenized for 60 s with a tissue Tissuemiser homogenizer. Acetic acid was added to each sample to a final concentration of 0.5 M and incubated at 4 °C overnight. Cellular debris was removed by centrifugation, and the supernatant analyzed for total protein, using a BCA assay kit (Pierce/ThermoFisher Scientific). The Sircol-soluble collagen assay kit (Biocolor Ltd., Carrickfergus, UK) was used to extract collagen from duplicate samples using 200 μL of supernatant and 800 μL of dye reagent according to the manufacturer's instructions. Similarly prepared collagen standards (10–50 μg) were run in parallel. Collagen pellets were washed twice with denatured alcohol and dried before suspension in alkali reagent. Absorbance at 555 nm was read on a plate reader (SpectroMax M5e, Molecular Devices Corp). Data were expressed as μg of soluble collagen per mg of total proteins.

ICP-OES analysis to determine Ce content in the mouse lung

The total Ce content of the lungs of mice exposed for 44 days was collected and rinsed three times with PBS. Subsequently, the lung tissues were homogenized for 60 s with a Tissuemiser tissue homogenizer (Fisher Scientific). The probe was washed with 500 μL of PBS, which was added to the homogenate. All the homogenates were transferred to Teflon containers and acidified with 5 mL of 100% ultrahigh-purity nitric acid and digested at 95 °C for 3 h before drying and redissolving in 5% nitric acid. After digestion, the elemental Ce concentration in each sample was determined by a Shimadzu ICP-OES based on a calibration curve established by a series of concentrations of Ce standard solution (0.01–10 ppm) and expressed as μg of Ce/mg of proteins.

Western blotting

Equivalent amounts of total proteins from each sample were separated on 4-20% SDS-PAGE gels and transferred onto polyvinylidene difluoride (PVDF) membrane using a Trans-blot SD semi-dry transfer cell (Bio-Rad, Hercules, CA, USA). The membranes were blocked with 5% non-fat dry milk (Santa Cruz Biotech, Dallas, TX, USA) for 1 h at room temperature, and then probed with primary antibodies overnight at 4°C, followed by incubation with HRP-linked secondary antibody (GE Healthcare, Piscataway, NJ). An ECL-Plus Kit (GE Healthcare) was used to detect the signals and the NIH Image J was employed to quantify the protein bands. The primary antibodies used in the study were

as follows: anti-SPHK1 (Proteintech, Rosemont, IL, USA), anti-EGR1 (Proteintech), anti-TGF-β1 (Abcam, Cambridge, UK), anti-pSmad2 (Cell Signaling Technology, Danvers, MA, USA), anti-Smad2 (Proteintech), anti-pSmad3 (Abcam), anti-Smad3 (Proteintech), and anti-GAPDH (GeneTex, Irvine, CA, USA).

Chromatin immunoprecipitation (ChIP)-qPCR

An EZ ChIP Chromatin Immunoprecipitation Kit (Millipore, Billerica, MA, USA) was used to perform the ChIP assays. Briefly, the cells were treated with 1% formaldehyde for 10 min at room temperature to form the protein-DNA complex. After washing with PBS twice, the cells were lysed in RIPA buffer and the DNA was broken into pieces by sonication. The chromatin fragments were immunoprecipitated with primary antibody against EGR1 or IgG overnight at 4°C. The purified DNA pellets were then used for qPCR analysis and the procedures for qPCR were performed as previously described [48].

Luciferase reporter assay

Luciferase reporter assays were performed as previously reported [48]. Wild-type TGF-β1 promoter reporter vector (TGF-β1_Prom, SwitchGear Genomics, Carlsbad, CA, USA) was co-transfected with EGR1 plasmid (pCMV6-EGR1) into BEAS-2B cells using the Lipofectamine 3000 (Invitrogen) transfection reagent according to the manufacturer's instructions. After 24 h, the relative luciferase activities were measured using a LightSwitch luciferase assay kit (Switchgear Genomics).

siRNA transfection

The cells were transfected with siEGR1 (Sigma-Aldrich) and siCTRL (Sigma-Aldrich) using the lipofectamine RNAiMAX reagent (Invitrogen) according to the manufacturer's instruction. After 24 h incubation, the siRNA medium was removed from the cells and replaced with fresh complete medium for subsequent experiments.

Immunofluorescence

Briefly, the cells were fixed with 4 % paraformaldehyde and then permeabilized with 0.1% Triton X-100. After incubating with immunostaining blocking buffer for 1 h at room temperature, the samples were probed with primary antibodies against PCNA (Proteintech), COL1A1 (Proteintech) and α-SMA (Abcam) at 4°C overnight, and subsequently with a fluorescence-conjugated secondary antibody at room temperature for 1 h. Images were captured using an inverted fluorescence microscope (Leica Microsystems, Wetzlar, Germany).

Statistical analysis

Statistical analysis was performed using the GraphPad Prism 9 software (GraphPad Software, La Jolla, CA, USA). All results were expressed as mean ± standard deviation unless otherwise stated. One-way ANOVA was used to compare the levels of metabolites among groups. Statistical significance thresholds were set as *$p < 0.05$; **$p < 0.01$; ***$p < 0.001$.

Supplementary Material

Refer to Web version on PubMed Central for supplementary material.

Acknowledgements

This work was supported, in part, by the California TRDRP Program (S.H.) and R01 HL139379 of National Heart, Lung, and Blood Institute (NHLBI) of the National Institutes of Health (T.X.). The authors thank the Molecular Screening Shared Resource (MSSR), the Flow Cytometry Core Facility of the Jonsson Comprehensive Cancer Center, and the Translational Pathology Core Laboratory (TPCL) Research Facility at UCLA.

References

[1]. Demirer GS, Zhang H, Matos JL, Goh NS, Cunningham FJ, Sung Y, Chang R, Aditham AJ, Chio L, Cho MJ, Staskawicz B, Landry MP, Nat Nanotechnol, 14 (2019) 456–464. [PubMed: 30804481]

[2]. Fratila RM, Rivera-Fernandez S, de la Fuente JM, Nanoscale, 7 (2015) 8233–8260. [PubMed: 25877250]

[3]. Shukla S, Eber FJ, Nagarajan AS, DiFranco NA, Schmidt N, Wen AM, Eiben S, Twyman RM, Wege C, Steinmetz NF, Adv Healthc Mater, 4 (2015) 874–882. [PubMed: 25641794]

[4]. Liang Z, Wang X, Yu G, Li M, Shi S, Bao H, Chen C, Fu D, Ma W, Xue C, Sun B, Nano Today, 43 (2022) 101445. [PubMed: 35261619]

[5]. Ridolfo R, Tavakoli S, Junnuthula V, Williams DS, Urtti A, van Hest JCM, Biomacromolecules, 22 (2021) 126–133. [PubMed: 32510218]

[6]. Lin S, Wang X, Ji Z, Chang CH, Dong Y, Meng H, Liao YP, Wang M, Song TB, Kohan S, Xia T, Zink JI, Lin S, Nel AE, ACS Nano, 8 (2014) 4450–4464. [PubMed: 24720650]

[7]. Ma JY, Mercer RR, Barger M, Schwegler-Berry D, Scabilloni J, Ma JK, Castranova V, Toxicol Appl Pharmacol, 262 (2012) 255–264. [PubMed: 22613087]

[8]. Reed K, Cormack A, Kulkarni A, Mayton M, Sayle D, Klaessig F, Stadler B, Environ. Sci.: Nano, 1 (2014) 390–405.

[9]. Ivanov VK, Shcherbakov AB, Usatenko AV, Russian Chemical Reviews, 78 (2009) 855–871.

[10]. Corma A, Atienzar P, Garcia H, Chane-Ching JY, Nat Mater, 3 (2004) 394–397. [PubMed: 15146175]

[11]. Jung H, Kittelson DB, Zachariah MR, Combustion and Flame, 142 (2005) 276–288.

[12]. Campbell CT, Peden CH, Science, 309 (2005) 713–714. [PubMed: 16051777]

[13]. Dhall A, Self W, Antioxidants (Basel), 7 (2018).

[14]. Hasin Y, Seldin M, Lusis A, Genome Biol, 18 (2017) 83. [PubMed: 28476144]

[15]. Zhang J, Pavlova NN, Thompson CB, EMBO J, 36 (2017) 1302–1315. [PubMed: 28420743]

[16]. Ghosh-Choudhary S, Liu J, Finkel T, Trends Cell Biol, 30 (2020) 201–212. [PubMed: 31983571]

[17]. Figlia G, Willnow P, Teleman AA, Dev Cell, 54 (2020) 156–170. [PubMed: 32693055]

[18]. Hu S, Wang J, Ji EH, Christison T, Lopez L, Huang Y, Anal Chem, 87 (2015) 6371–6379. [PubMed: 25973679]

[19]. Cui L, Zhao X, Jin Z, Wang H, Yang SF, Hu S, J Pineal Res, 71 (2021) e12767. [PubMed: 34533844]

[20]. Cui L, Liu J, Yan X, Hu S, Anal Chem, 89 (2017) 11737–11743. [PubMed: 28972752]

[21]. Marques MRC, Loebenberg R, Almukainzi M, Dissolution Technologies, 18 (2011) 15–28.

[22]. Ji Z, Wang X, Zhang H, Lin S, Meng H, Sun B, George S, Xia T, Nel AE, Zink JI, ACS Nano, 6 (2012) 5366–5380. [PubMed: 22564147]

[23]. Meng XM, Nikolic-Paterson DJ, Lan HY, Nat Rev Nephrol, 12 (2016) 325–338. [PubMed: 27108839]

[24]. Kim KK, Sheppard D, Chapman HA, Cold Spring Harb Perspect Biol, 10 (2018).

[25]. Frangogiannis N, J Exp Med, 217 (2020) e20190103. [PubMed: 32997468]

[26]. Proia RL, Hla T, J Clin Invest, 125 (2015) 1379–1387. [PubMed: 25831442]

[27]. Pyne NJ, Pyne S, Nat Rev Cancer, 10 (2010) 489–503. [PubMed: 20555359]

[28]. Obinata H, Hla T, Int Immunol, 31 (2019) 617–625. [PubMed: 31049553]

[29]. Kowalski GM, Carey AL, Selathurai A, Kingwell BA, Bruce CR, PLoS One, 8 (2013) e72449. [PubMed: 24039766]

[30]. Huang LS, Sudhadevi T, Fu P, Punathil-Kannan PK, Ebenezer DL, Ramchandran R, Putherickal V, Cheresh P, Zhou G, Ha AW, Harijith A, Kamp DW, Natarajan V, Int J Mol Sci, 21 (2020).

[31]. Ebenezer DL, Fu P, Natarajan V, Pharmacol Ther, 168 (2016) 143–157. [PubMed: 27621206]

[32]. Li R, Ji Z, Dong J, Chang CH, Wang X, Sun B, Wang M, Liao YP, Zink JI, Nel AE, Xia T, ACS Nano, 9 (2015) 3293–3306. [PubMed: 25727446]

[33]. Grossgarten M, Holzlechner M, Vennemann A, Balbekova A, Wieland K, Sperling M, Lendl B, Marchetti-Deschmann M, Karst U, Wiemann M, Part Fibre Toxicol, 15 (2018) 31. [PubMed: 30012173]

[34]. Wang X, Xia T, Duch MC, Ji Z, Zhang H, Li R, Sun B, Lin S, Meng H, Liao YP, Wang M, Song TB, Yang Y, Hersam MC, Nel AE, Nano Lett, 12 (2012) 3050–3061. [PubMed: 22546002]

[35]. Wang X, Duch MC, Mansukhani N, Ji Z, Liao YP, Wang M, Zhang H, Sun B, Chang CH, Li R, Lin S, Meng H, Xia T, Hersam MC, Nel AE, ACS Nano, 9 (2015) 3032–3043. [PubMed: 25646681]

[36]. Wang X, Mansukhani ND, Guiney LM, Ji Z, Chang CH, Wang M, Liao YP, Song TB, Sun B, Li R, Xia T, Hersam MC, Nel AE, Small, 11 (2015) 5079–5087. [PubMed: 26237579]

[37]. Wang X, Lee JH, Li R, Liao YP, Kang J, Chang CH, Guiney LM, Mirshafiee V, Li L, Lu J, Xia T, Hersam MC, Nel AE, Small, 14 (2018) e1703915. [PubMed: 29733549]

[38]. Xia T, Zhao Y, Sager T, George S, Pokhrel S, Li N, Schoenfeld D, Meng H, Lin S, Wang X, Wang M, Ji Z, Zink JI, Madler L, Castranova V, Lin S, Nel AE, ACS Nano, 5 (2011) 1223–1235. [PubMed: 21250651]

[39]. Zhang H, Pokhrel S, Ji Z, Meng H, Wang X, Lin S, Chang CH, Li L, Li R, Sun B, Wang M, Liao YP, Liu R, Xia T, Madler L, Nel AE, J Am Chem Soc, 136 (2014) 6406–6420. [PubMed: 24673286]

[40]. Naatz H, Lin S, Li R, Jiang W, Ji Z, Chang CH, Koser J, Thoming J, Xia T, Nel AE, Madler L, Pokhrel S, ACS Nano, 11 (2017) 501–515. [PubMed: 28026936]

[41]. Sun B, Wang X, Liao YP, Ji Z, Chang CH, Pokhrel S, Ku J, Liu X, Wang M, Dunphy DR, Li R, Meng H, Madler L, Brinker CJ, Nel AE, Xia T, ACS Nano, 10 (2016) 8054–8066. [PubMed: 27483033]

[42]. Sun B, Pokhrel S, Dunphy DR, Zhang H, Ji Z, Wang X, Wang M, Liao YP, Chang CH, Dong J, Li R, Madler L, Brinker CJ, Nel AE, Xia T, ACS Nano, 9 (2015) 9357–9372. [PubMed: 26200133]

[43]. Dumitrescu E, Wallace K, Andreescu S, Methods Mol Biol, 1894 (2019) 331–343. [PubMed: 30547471]

[44]. Wu T, Xu H, Liang X, Tang M, Chemosphere, 221 (2019) 708–726. [PubMed: 30677729]

[45]. Cui L, Wang X, Sun B, Xia T, Hu S, ACS Nano, 13 (2019) 13065–13082. [PubMed: 31682760]

[46]. Wang X, Xia T, Ntim SA, Ji Z, Lin S, Meng H, Chung CH, George S, Zhang H, Wang M, Li N, Yang Y, Castranova V, Mitra S, Bonner JC, Nel AE, ACS Nano, 5 (2011) 9772–9787. [PubMed: 22047207]

[47]. Wang X, Liao YP, Telesca D, Chang CH, Xia T, Nel AE, Small, 13 (2017).

[48]. Huang J, Ji EH, Zhao X, Cui L, Misuno K, Guo M, Huang Z, Chen X, Hu S, J Exp Clin Cancer Res, 38 (2019) 138. [PubMed: 30922366]

Highlights

- LC-MS-based metabolomics is a sensitive methodology for the assessment of nanotoxicity. *In vitro* metabolomic analysis may be used for predicting the nanotoxicity *in vivo*.
- A number of metabolites in the cellular metabolic pathways of S1P, fatty acid oxidation and inflammation were significantly altered by CeO_2 NPs, especially those with high aspect ratios.
- CeO_2 NPs promote mouse lung fibrosis in an aspect ratio dependent manner through the TGF-β1/SPHK1/S1P pathway in addition to the conventional TGF-β1-SMAD pathway.

A

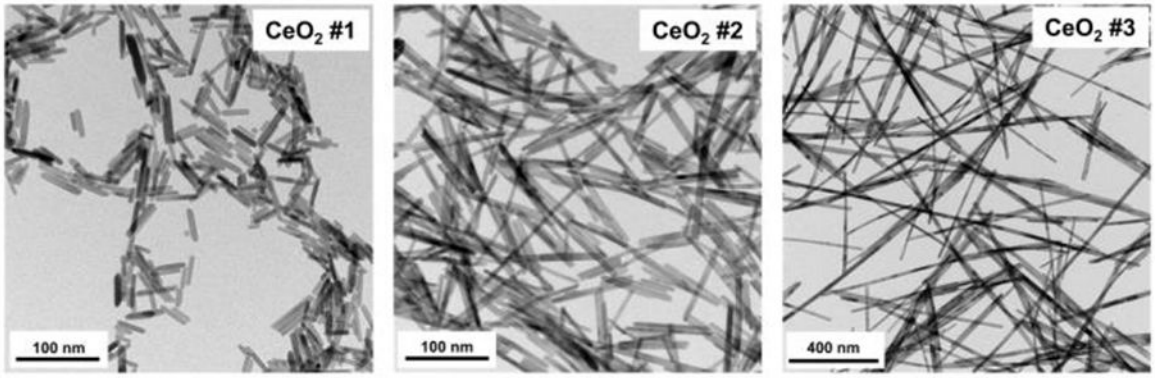

B

	Length (nm)	Diameter (nm)	Aspect ratio	Hydrodynamic size (nm)		Zeta-potential (mV)	
				DI H_2O	Complete cell culture medium	DI H_2O	Complete cell culture medium
CeO_2 #1	48.1 ± 11.7	6.5±0.6	7.2±1.6	231.4 ± 12.0	578.1 ± 97.8	-28.7 ± 1.1	-11.1 ± 2.6
CeO_2 #2	495.4 ± 81.2	9.5±0.8	52.1±8.3	651.3 ± 72.1	749.3 ± 116.5	-23.4 ± 3.7	-15.3 ± 1.3
CeO_2 #3	1197.2 ± 203.7	9.5±0.9	126.0 ± 21.3	978.8 ± 85.5	776.5 ± 93.4	-31.6 ± 1.9	-9.7 ± 0.7

C

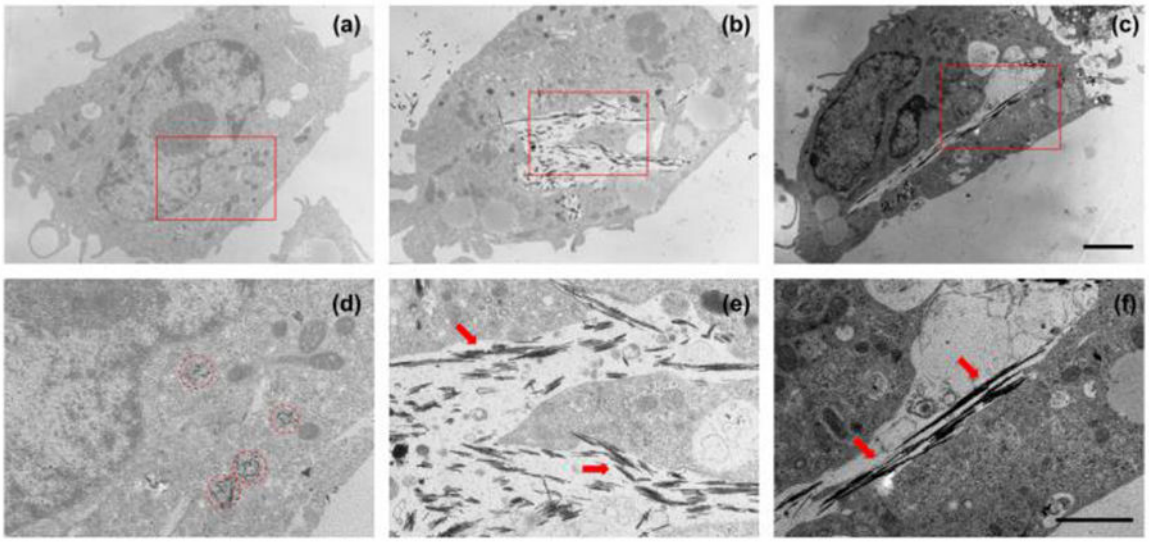

Figure 1.

Physicochemical characterization of CeO_2 NPs. (A) The morphology of CeO_2 #1, CeO_2 #2, and CeO_2 #3 was analyzed by transmission electron microscopy (TEM). (B) The particle size and ζ-potential of the CeO_2 NPs in deionized water. (C) Ultrastructural images to depict the interaction of CeO_2 nanorods/nanowires with BEAS-2B cells using TEM. BEAS-2B cells were cultured with CeO_2 nanorods/nanowires in BEGM for 24 h at 25 μg/mL. CeO_2 # 1 (a, d); CeO_2 # 2 (b, e); CeO_2 # 3 (c, f). Panels d, e, and f show a higher magnification view of the labeled square area in panels a, b, and c, respectively. The circles in panels a/d

highlight the CeO_2 # 1 nanorods taken up into membrane-lined subcelluar compartments. Scale bar for panels a, b and c = 2 μm; scale bar for panels d, e and f = 1 μm.

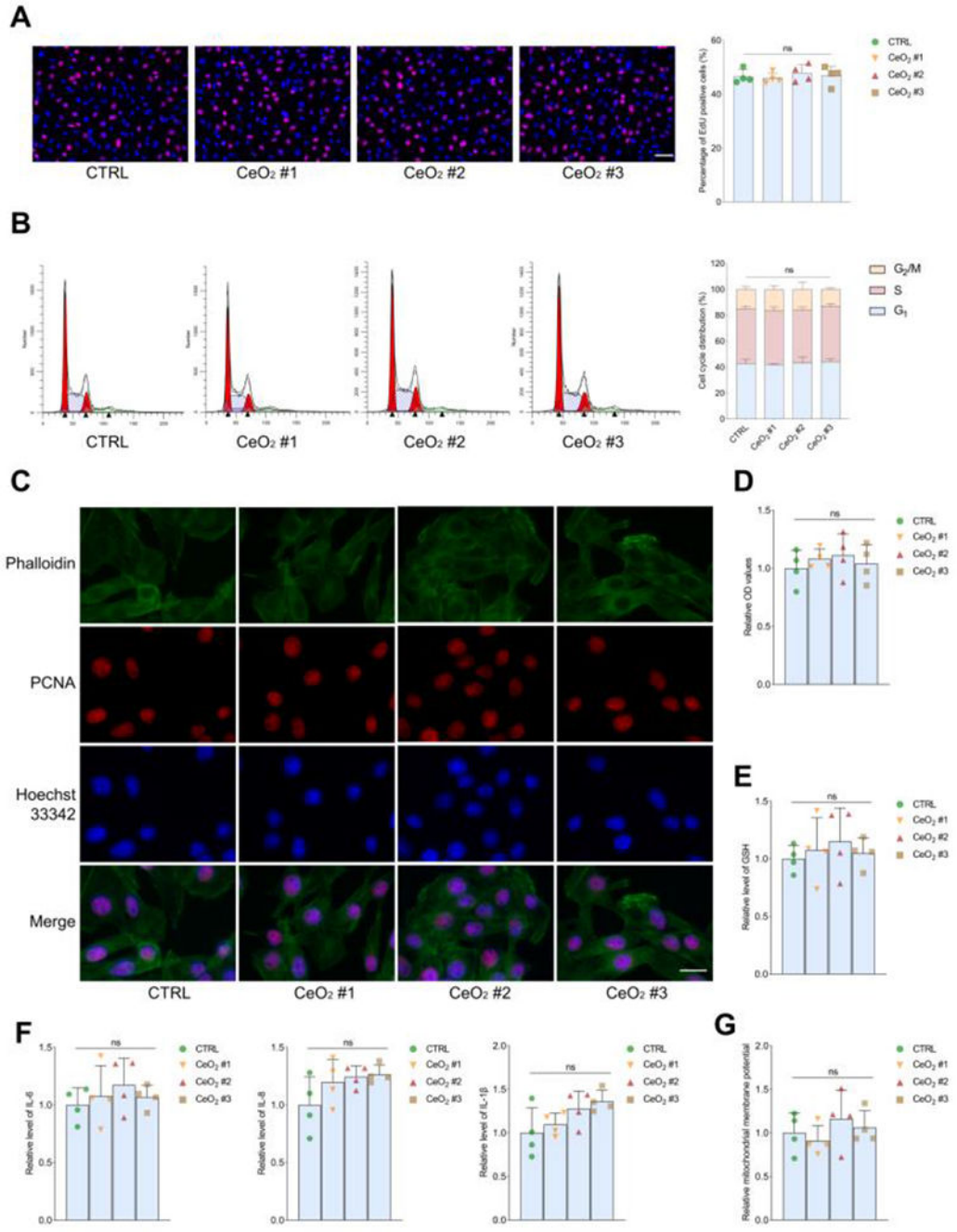

Figure 2.

Cell-based functional assays of untreated BEAS-2B cells (CTRL) and the BEAS-2B cells treated with three types of CeO_2 NPs. (A) The percentage of EdU positivity of untreated and CeO_2 NP-treated BEAS-2B cells (scale bar=50 μm). (B) The cell cycle distribution of untreated and CeO_2 NP-treated BEAS-2B cells. (C) The immunofluorescence intensity of PCNA in untreated and CeO_2 NP-treated BEAS-2B cells (scale bar=20 μm). (D) MTS assays of untreated and CeO_2 NP-treated BEAS-2B cells. (E) The GSH levels in untreated and CeO_2 NP-treated BEAS-2B cells. (F) The levels of IL-6, IL-8 and IL-1β in untreated

and CeO_2 NP-treated BEAS-2B cells. (G) The relative mitochondria potential in untreated and CeO_2 NP-treated BEAS-2B cells.

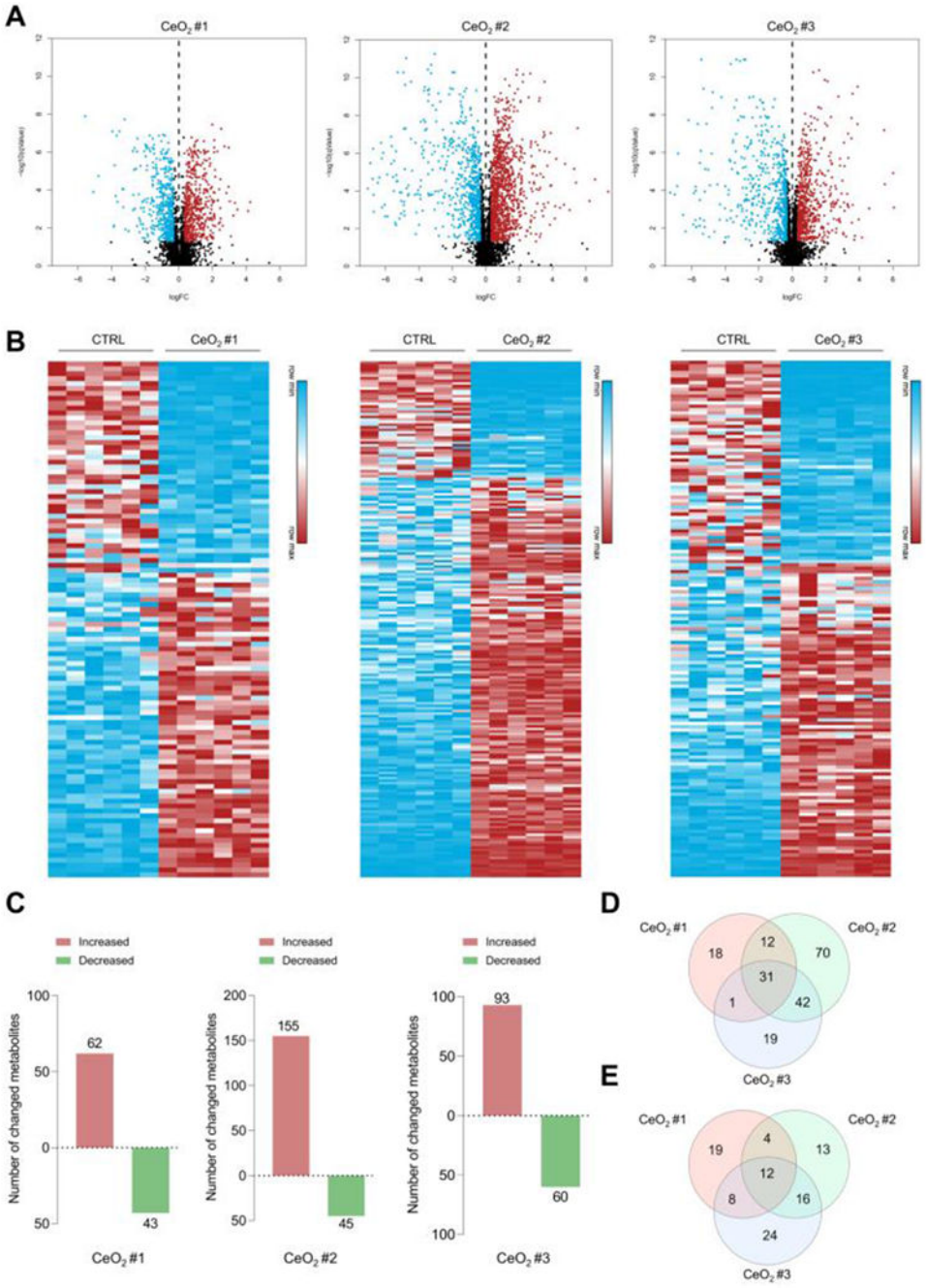

Figure 3.

Metabolomic analysis of the BEAS-2B cells exposed to different types of CeO_2 NPs (high dose, 25 μg/mL). (A) Volcano plots of the significantly altered metabolic features between CeO_2 NP treated and untreated (CTRL) cells (n=6 per group). (B) Heat maps of differentially expressed metabolites between CeO_2 NP treated and untreated cells (n=6 per group). (C) The number of identified metabolites with significant changes between CeO_2 NP treated and untreated cells. (D) The number of commonly and differentially altered metabolites in the BEAS-2B cells treated with different types of CeO_2 NPs.

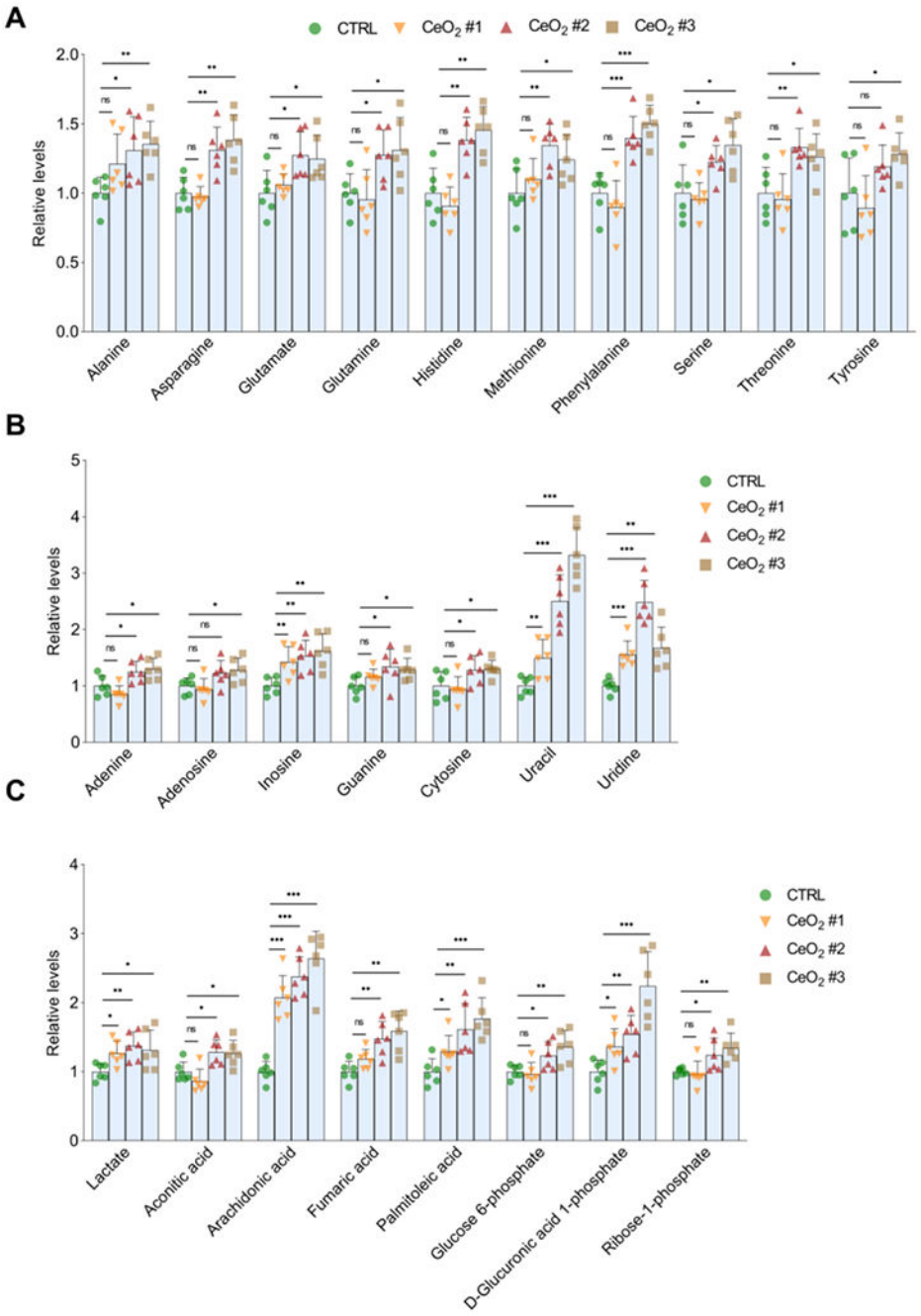

Figure 4.

The changes of representative metabolites in the BEAS-2B cells exposed to CeO_2 NPs. (A) The alterations of amino acids in the BEAS-2B cells treated with different types of CeO_2 NPs. (B) The altered levels of representative nucleosides/nucleotides in the BEAS-2B cells exposed to CeO_2 NPs. (C) The altered levels of representative organic acid metabolites in the BEAS-2B cells exposed to CeO_2 NPs.

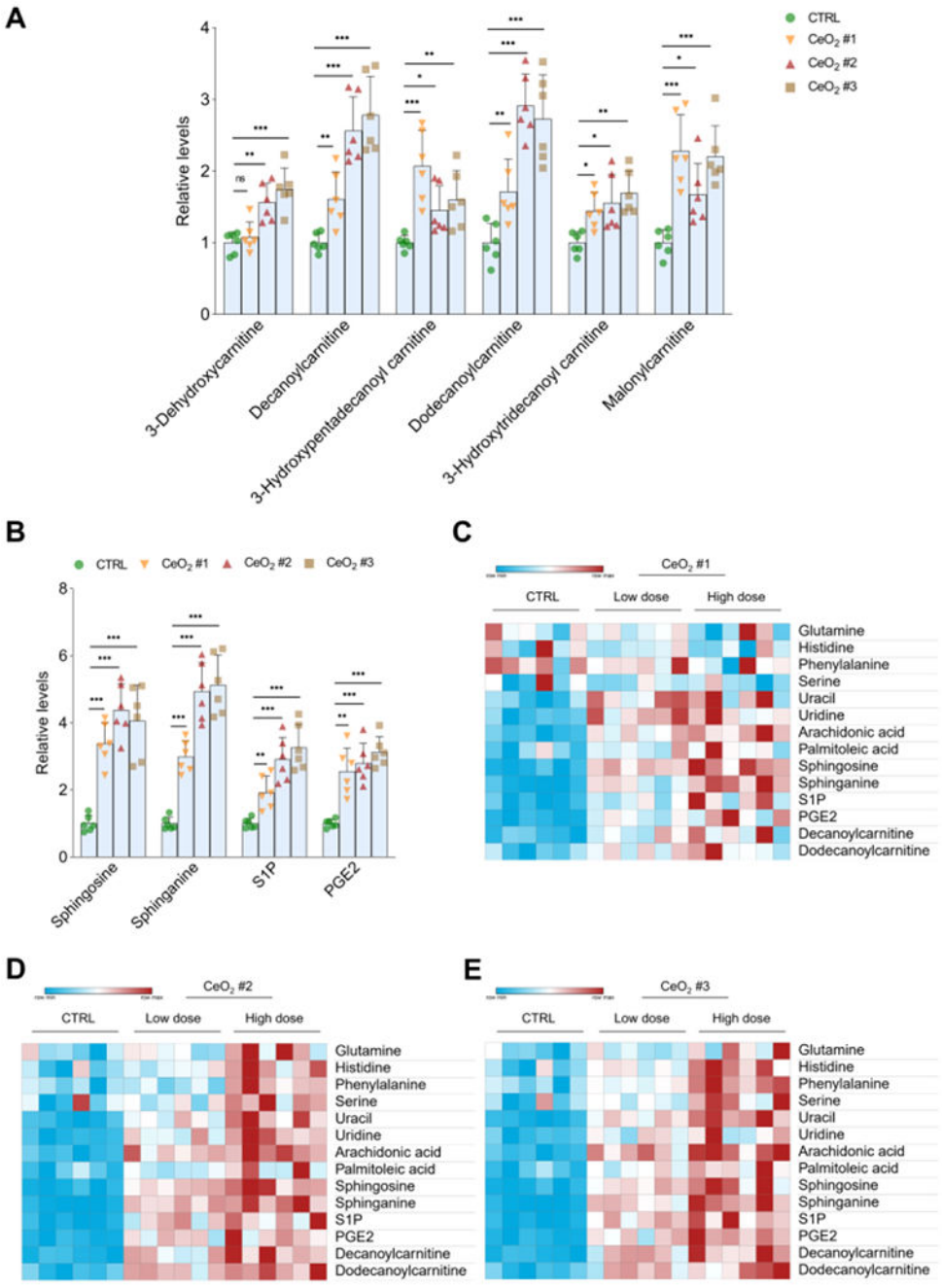

Figure 5.

The changes of acylcarnitines, PGE2 and metabolites in S1P pathway in the BEAS-2B cells exposed to CeO_2 NPs. (A) The altered levels of acylcarnitines in cells treated with different types of CeO_2 NPs. (B) The alteration of PGE2 and metabolites in S1P pathway in the BEAS-2B cells exposed to CeO_2 NPs. (C-E) The heatmaps revealed that most of the representative metabolites were altered by CeO_2 NPs with different aspect ratios in a dose-dependent manner (high dose: 25 μg/mL; low dose: 12.5 μg/mL).

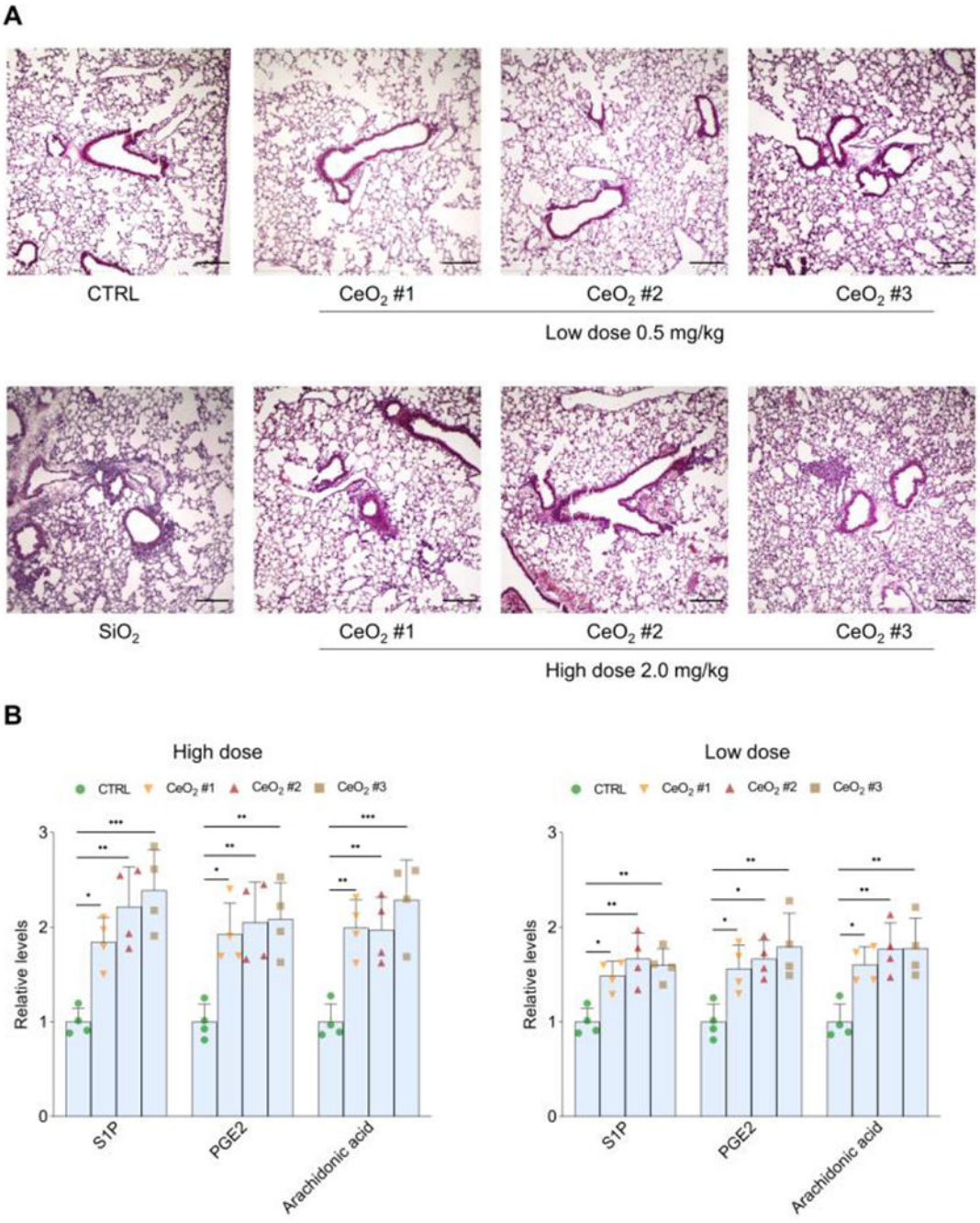

Figure 6.

Validation of the changes in representative metabolites in the mouse models upon acute exposures (40 h) to CeO_2 NPs. (A) H&E staining of the lung tissues from the mice exposed to the three types of CeO_2 NPs with high (2.0 mg/kg) or low dose (0.5 mg/kg) (scale bar=200 μm). (B) Enzymatic assays of S1P, PGE2 and arachidonic acid in the lung tissues of the mice exposed to the CeO_2 NPs with high or low doses.

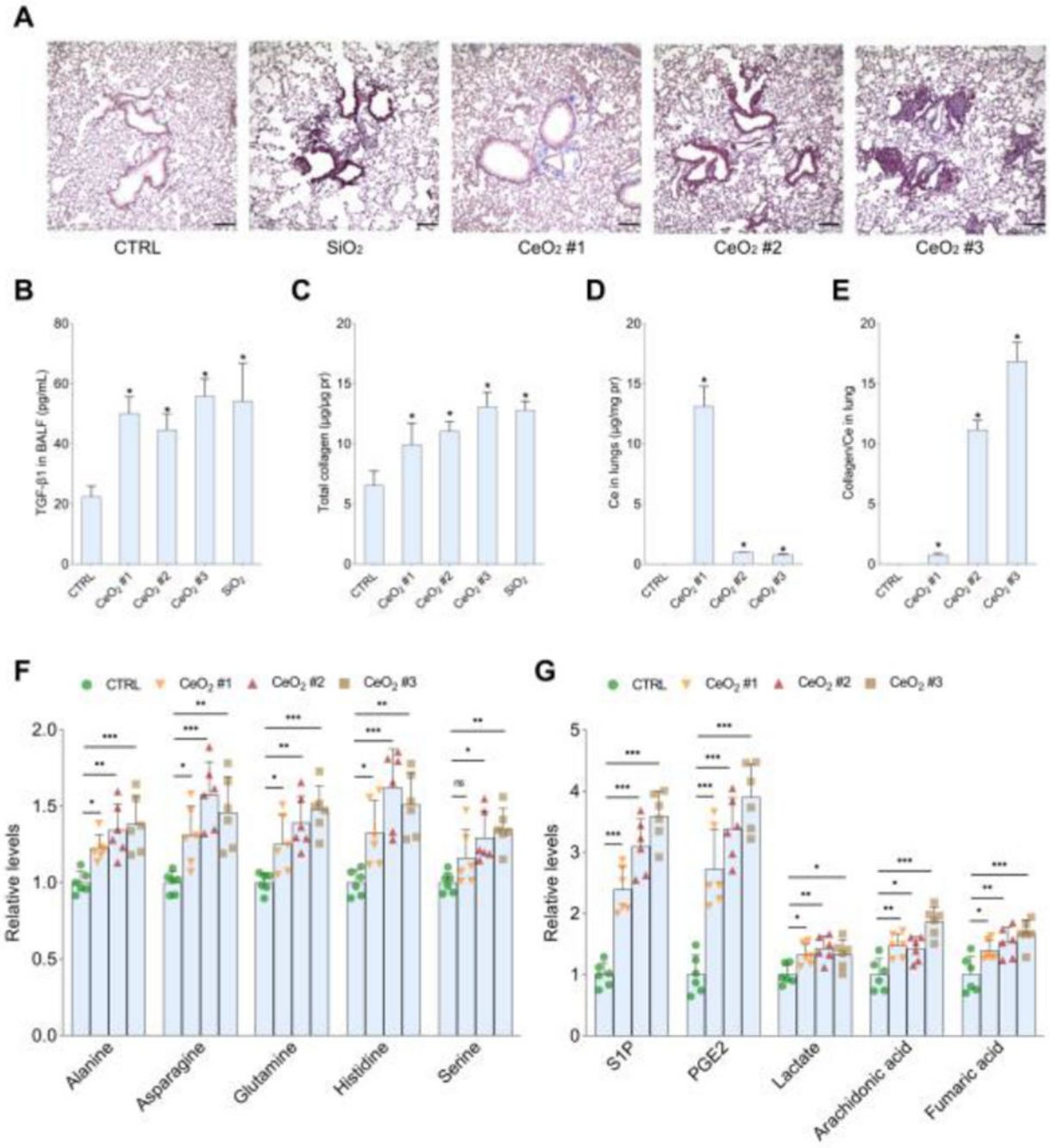

Figure 7.

Lung fibrosis induced by chronic exposures (44 days, high dose, 2.0 mg/kg) to CeO_2 NPs and validation of the changes in representative metabolites. (A) Masson's trichrome staining of the lung tissues from the mice with indicated treatments (CeO_2 NPs #1, CeO_2 NPs #1, CeO_2 NPs #1 and positive control SiO_2 NPs) (scale bar = 200 μm). (B) The levels of TGF-β1 in the BALF from the mice exposed to CeO_2 NPs with different aspect ratios. (C) The amount of total collagen in the lung tissues from the mice with indicated treatments. (D) The amount of CeO_2 NPs in the lung tissues from the mice exposed to CeO_2 NPs with

different aspect ratios. (E) The ratio of collagen/CeO_2 NPs in the lung tissues with indicated treatments. (F-G) Enzymatic assays of alanine, asparagine, glutamine, histidine, serine, S1P, PGE2, lactate, arachidonic acid and fumaric acid in the lung tissues from the mice exposed to CeO_2 NPs.

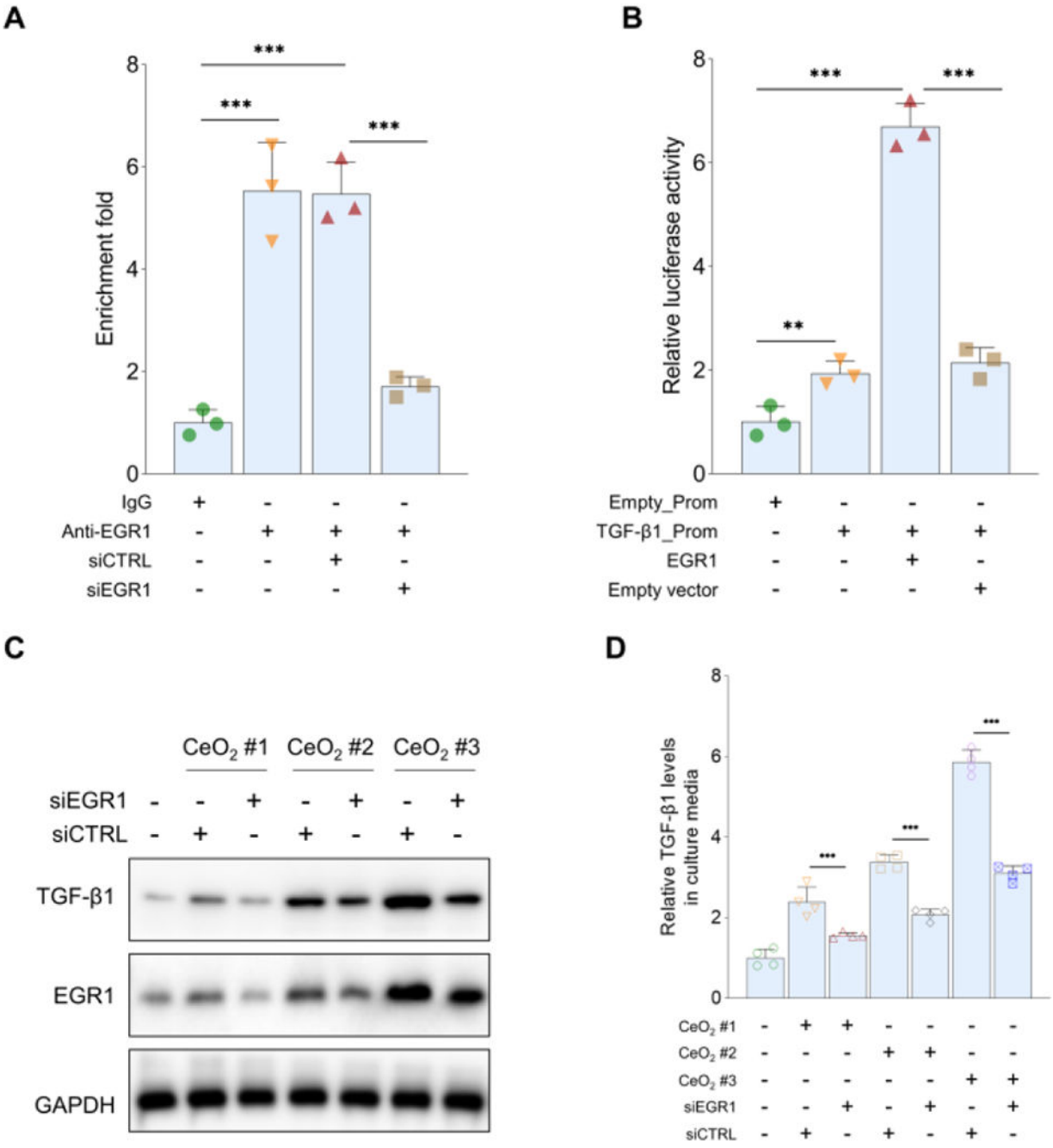

Figure 8.

EGR1 is a upstream regulator of TGF-β1 in CeO_2 NP treated BEAS-2B cells. (A) EGR1 was enriched in the promoter region of TGF-β1, and knockdown of EGR1 significantly reduced its enrichment. (B) Luciferase reporter assays indicated that EGR1 directly induced the promoter activity of TGF-β1 in the BEAS-2B cells. (C) Both TGF-β1 and EGR1 were increased by CeO_2 NPs in an aspect ratio dependent manner, and EGR1 depletion suppressed the expression of TGF-β1. (D) EGR1 downregulation significantly decreased

the levels of TGF-β1 in the culture media derived from the BEAS-2B cells with indicated treatments.

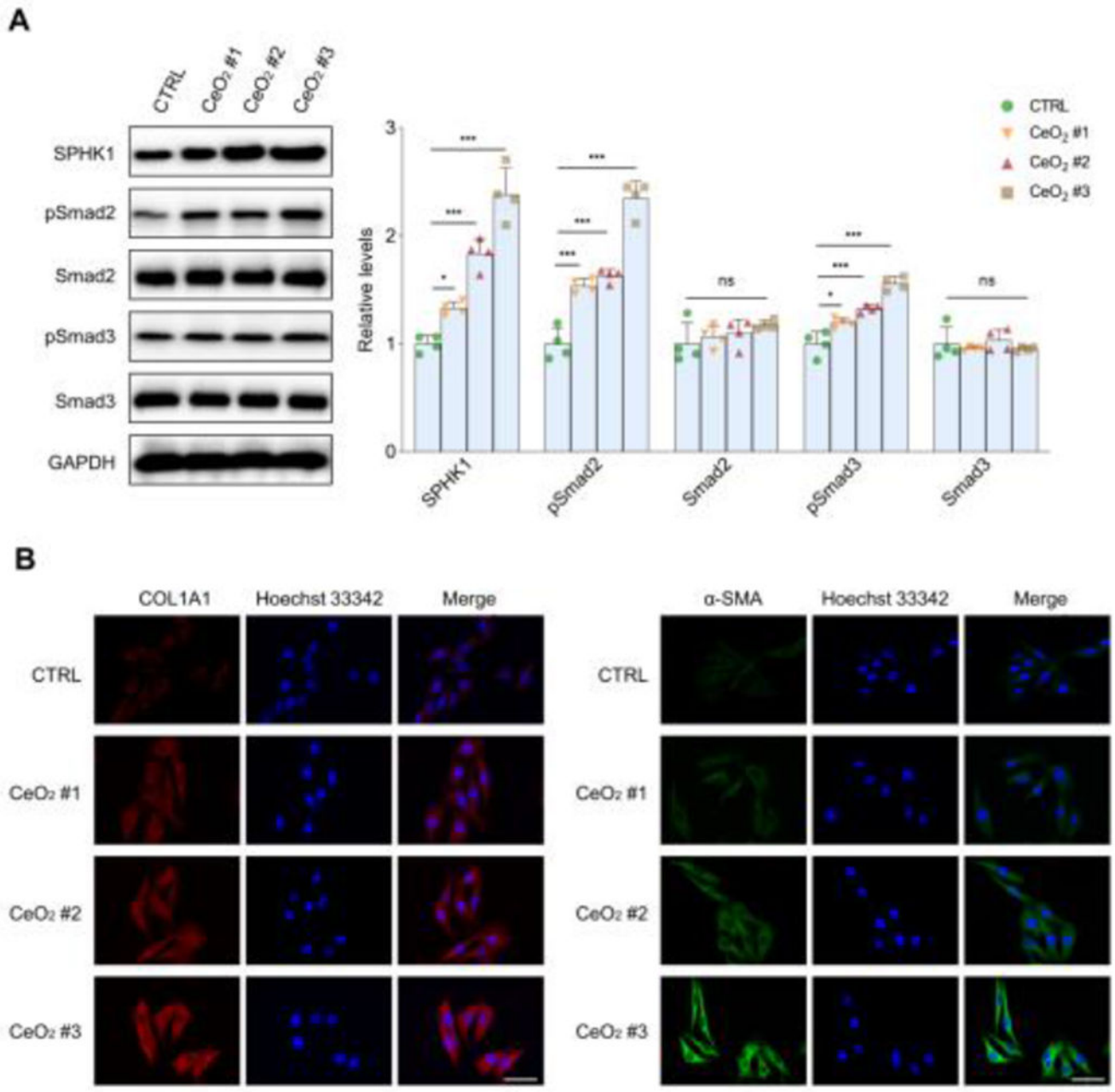

Figure 9.

CeO_2 NPs induced the expression of SPHK1, pSmad2, pSmad3 and fibrosis markers COL1A1 and α-SMA in BEAS-2B cells. (A) Western blot analysis of the expression of SPHK1, pSmad2, Smad2, pSmad3 and Smad3 in the BEAS-2B cells exposed to CeO_2 NPs. (B) Immunofluorescence of COL1A1 and α-SMA in the BEAS-2B cells exposed to different types of CeO_2 NPs (scale bar=50 μm).

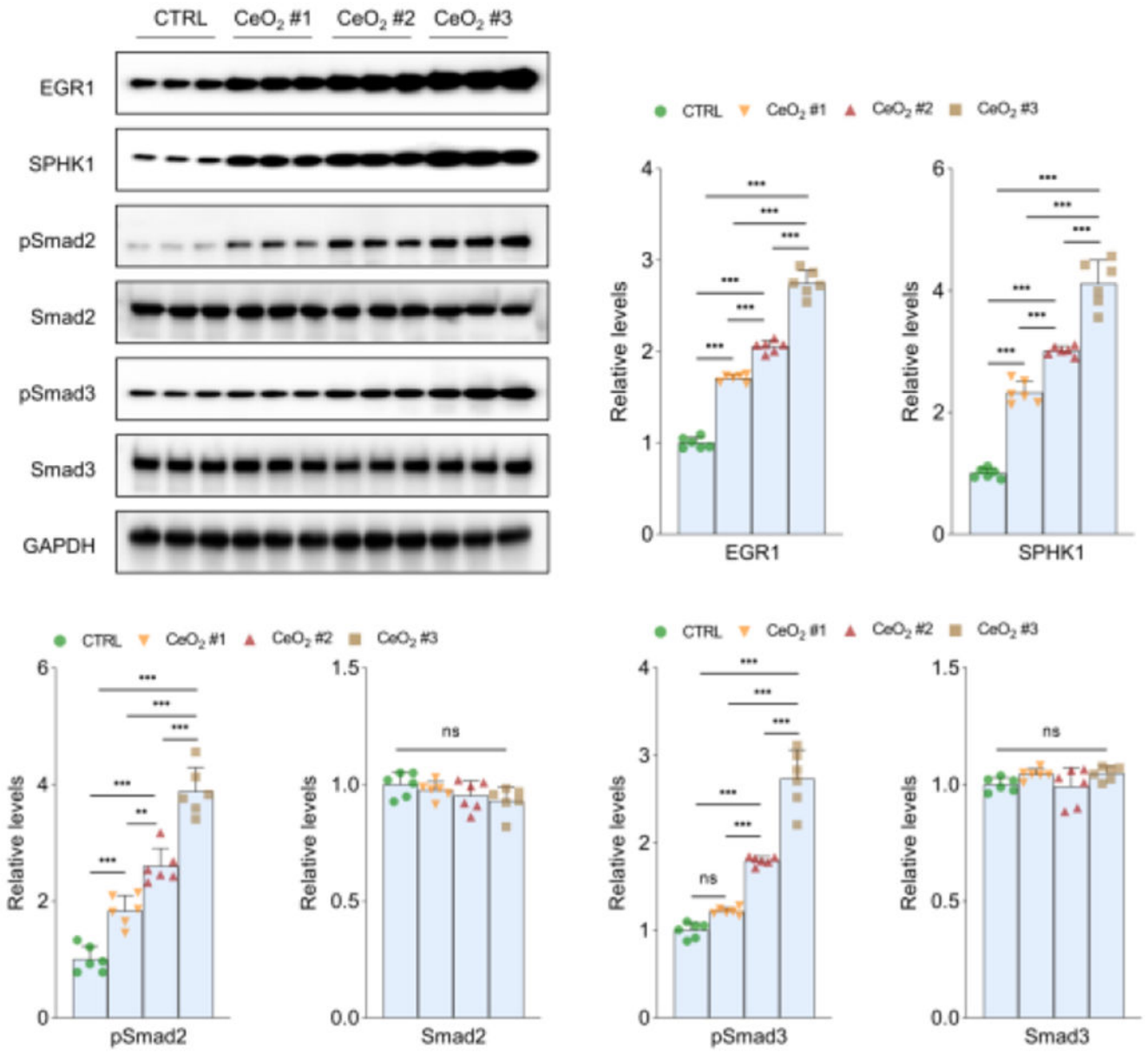

Figure 10.

As indicated by Western blot analysis, the expression of EGR1, SPHK1, pSmad2 and pSmad3 were significantly increased in the lung tissues of the mice upon chronic exposures (44 days, high dose, 2.0mg/kg) to CeO_2 NPs in an aspect ratio dependent manner.

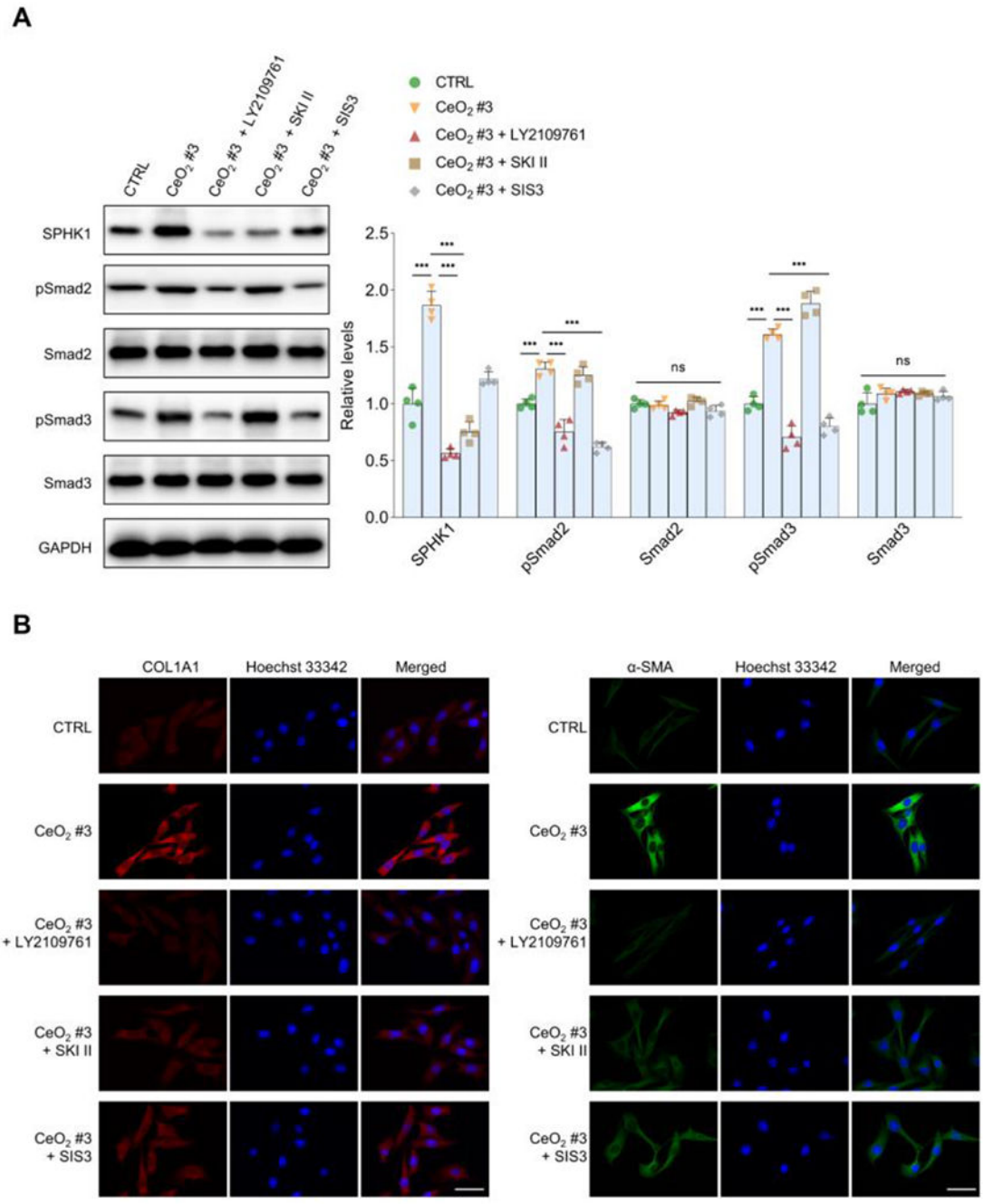

Figure 11.

SPHK1-S1P pathway exhibited a greater effect on the TGF-β1-mediated lung fibrosis compared to the conventional Smad2/3 pathway. (A) Blocking the interaction between TGF-β1 and TGFBR suppressed the expression of SPHK1 and phosphorylation of Smad2 and Smad3. As expected, SPHK1 inhibtor SKI II significantly decreased SPHK level and the Smad3 inhibitor SIS3 dramatically reduced the levels of pSmad2 and pSmad3 in BEAS-2B cells. The protein expression levels were measured by Western blotting. (B) Targeting TGFBR almost completely obliterated the fibrosis-enhancing effects of CeO_2 NPs, and

targeting SPHK1 exhibited a more attenuation effect on the expression of COL1A and α-SMA, when compared to targeting Smad3 phosphorylation (scale bar=50 μm).

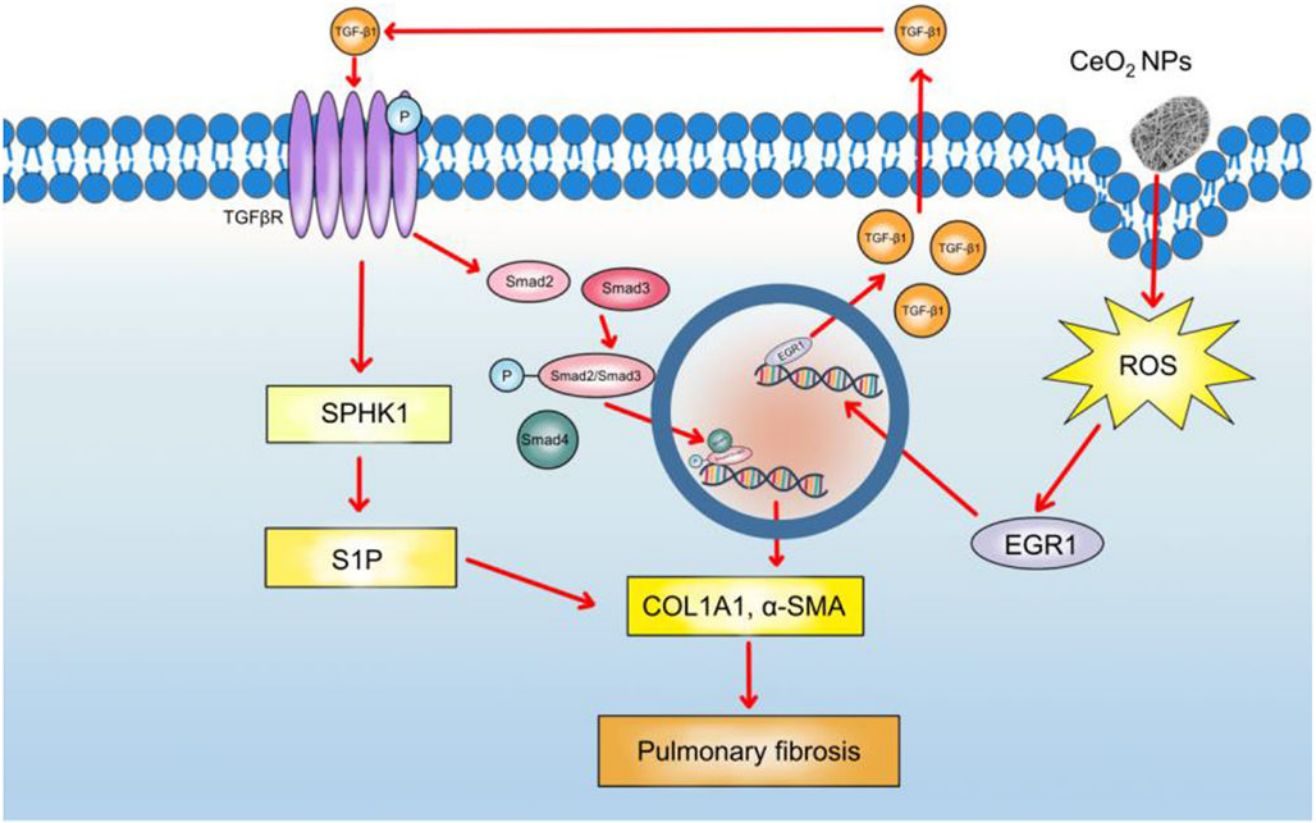

Figure 12.

A schematic diagram illustrating the proposed mechanism for CeO_2 NP-induced lung fibrosis.